Journal of Hazardous Materials 192 (2011) 1515–1524

Contents lists available at ScienceDirect

Journal of Hazardous Materials

journal homepage: www.elsevier.com/locate/jhazmat

Removal of methylene blue from aqueous solution by a solvothermal-synthesized graphene/magnetite composite

Lunhong Ai[a,b,*], Chunying Zhang[b], Zhonglan Chen[a,b]

[a] Chemical Synthesis and Pollution Control Key Laboratory of Sichuan Province, Nanchong 637002, Sichuan, PR China
[b] College of Chemistry and Chemical Engineering, China West Normal University, Shida Road 1#, Nanchong 637002, PR China

ARTICLE INFO

Article history:
Received 4 April 2011
Received in revised form 29 May 2011
Accepted 26 June 2011
Available online 1 July 2011

Keywords:
Graphene
Magnetite
Composite
Adsorption
Methylene blue

ABSTRACT

In this study, we have demonstrated a facile one-step solvothermal method for the synthesis of the graphene nanosheet (GNS)/magnetite (Fe_3O_4) composite. During the solvothermal treatment, *in situ* conversion of $FeCl_3$ to Fe_3O_4 and simultaneous reduction of graphene oxide (GO) into graphene in ethylene glycol solution were achieved. Electron microscopy study suggests the Fe_3O_4 spheres with a size of about 200 nm are uniformly distributed and firmly anchored on the wrinkled graphene layers with a high density. The resulting GNS/Fe_3O_4 composite shows extraordinary adsorption capacity and fast adsorption rates for removal of organic dye, methylene blue (MB), in water. The adsorption kinetics, isotherms and thermodynamics were investigated in detail to reveal that the kinetics and equilibrium adsorptions are well-described by pseudo-second-order kinetic and Langmuir isotherm model, respectively. The thermodynamic parameters reveal that the adsorption process is spontaneous and endothermic in nature. This study shows that the as-prepared GNS/Fe_3O_4 composite could be utilized as an efficient, magnetically separable adsorbent for the environmental cleanup.

1. Introduction

Graphene, a novel one-atom-thick two-dimensional graphitic carbon system, is a rising star on the horizon of materials science and condensed matter physics [1,2]. Owing to the fascinating mechanical, electrical, thermal and optical properties, and potential application in nanoelectronics, sensors, catalysis, batteries, supercapacitors and transistors, graphene has received intensive attention in recent years [3,4]. In comparison to carbon nanotubes (CNTs), graphene has the perfect sp^2 hybrid carbon nanostructure and the higher specific surface area, which can be easily obtained from natural graphite via a facile chemical oxidation–exfoliation–reduction procedure at a low cost [5,6]. Moreover, through the chemical oxidation modification, abundant oxygen-containing functional groups appear in graphene oxide (GO) and reduced graphene oxide [7–9]. This unique surface property enables them as ideal substrates to anchor inorganic nanoparticles (NPs) for enhancement of wider applications. For example, a large number of recent works have shown lithium ion battery and supercapacitor applications of oxides coupled with graphene [10–12]. The incorporation of graphene can significantly improve the electrochemical activity of oxides. Also, the combination of common photocatalysts (e.g. TiO_2, ZnO, $BiVO_4$ and Bi_2WO_6, etc.) and graphene could lead to the enhancement of adsorptivity of pollutants, light absorption intensity, electron hole pairs lifetime, and extended light absorption range, which may open up new opportunities in next generation photocatalyst systems [13–16].

Magnetite (Fe_3O_4) NPs have drawn considerable attention because of the fundamental scientific interest and the promising applications in magnetic fluids, catalysis, sensors, biomedicine, spintronics, magnetic recording devices, and environmental remediation [17,18]. Additionally, Fe_3O_4 NPs also show advantages such as low toxicity, low cost, and eco-friendliness. Thus, the combination of graphene with magnetic NPs to produce a magnetic graphene-based composite would provide a new, functional hybrid with synergistic or complementary behavior between each constituent, and thus will have great advantages for above-mentioned applications. In particular, the magnetic NPs in such composite system could also serve as a stabilizer against the aggregation of individual graphene sheets due to a strong van der Waals interaction between graphene layers. Recently, the anticipated unique properties and wide applications of the graphene–Fe_3O_4 composite have been explored [19–25]. For instance, for lithium ion battery application, the graphene nanosheets could act not only as lithium storage active materials, but also as an electronically conductive matrix to improve the electrochemical performance of Fe_3O_4 [19]. Chen and co-workers [20] fabricated and demonstrated a magnetic-controlled conductive switch using the flexible

* Corresponding author. Tel.: +86 817 2568081; fax: +86 817 2224217.
E-mail address: ah_aihong@163.com (L. Ai).

0304-3894/$ – see front matter © 2011 Elsevier B.V. All rights reserved.
doi:10.1016/j.jhazmat.2011.06.068

and multifunctional graphene/Fe_3O_4 hybrid papers. He and Gao [21] found that the multifunctional graphene/Fe_3O_4 hybrid sheets showed the integrated properties of strong supraparamagnetism, electrical conductivity, highly chemical reactivity, good solubility, and excellent processability, which had a potential application in magnetic resonance imaging (MRI) technology. Zhou et al. [22] reported graphene/Fe_3O_4 composites were suitable for the immobilization and delivery of drugs, which presented high loading capacities of doxorubicin hydrochloride (DOX) due to appearance of π–π interactions between the quinone portion of DOX and the basal plane of graphene.

Recently, adsorption technology has been developed to solve environmental problems, which is a reliable alternative due to its simplicity, high efficiency, ease of operation as well as the availability of a wide range of adsorbents [26–40]. It has been shown previously that the composites of magnetic oxides and carbon materials, including activated carbon [41,42] and CNTs [43,44], had an excellent ability to remove toxic pollutants from water, and usually showed rapid adsorption rates, high adsorption capacities, and convenient magnetic separation. In this regard, the graphene/magnetic oxide composite was thereby spread to the field of water treatment. Till now, the adsorptive removal of arsenic and heavy metal in water on this kind of composite has been demonstrated [45,46]. Despite these advances, we try to understand the adsorption mechanism of the typical organic dye pollutants on the graphene/Fe_3O_4 composite. In this work, we report a facile, one-step solvothermal approach toward the synthesis of the graphene/Fe_3O_4 composite by *in situ* conversion of $FeCl_3$ to Fe_3O_4 and simultaneous reduction of GO into graphene in ethylene glycol solution. The kinetic and thermodynamic of the dye adsorption on the graphene/Fe_3O_4 composite have been investigated. The resulting graphene/Fe_3O_4 composite could be utilized as a magnetically separable and efficient adsorbent for dye removal from water.

2. Experimental

2.1. Materials

$FeCl_3{\cdot}6H_2O$, sodium acetate (NaAc), graphite powder, activated carbon (AC) powder, ethylene glycol (EG), methylene blue (MB) were purchased from Sinopharm Chemical Reagent Co., Ltd. (Shanghai, China) and used without further purification. All chemicals used in this study were of commercially available analytical grade. Multi-walled carbon nanotubes (MWCNTs, length: 5 μm; diameter: 50–90 nm; purity: >90%) purchased from Shenzhen Nanotech Port Ltd. Co. (Shenzhen, China). MWCNTs were purified via being dispersed in concentrated nitric acid at 60 °C with constant stirring for 12 h, followed by filtering and washing with distilled water several times until the pH value reached neutral, and then filtered and dried in vacuum at 60 °C for further use.

2.2. Preparation of graphene oxide (GO)

GO was synthesized from natural graphite powder by a modified Hummers method [47]. In a typical procedure, 120 mL of concentrated H_2SO_4 was added into a 500 mL flask containing 5 g of graphite and 2.5 g of $NaNO_3$ and followed by stirring for 30 min inside an ice bath. Then 15 g of $KMnO_4$ was added slowly to the mixture. The rate of addition was carefully controlled to keep the reaction temperature below 20 °C. The mixture was stirred at room temperature overnight. Then, 150 mL of H_2O was slowly added under vigorous stirring. The reaction temperature rapidly increased to 98 °C with effervescence, and the mixture color changed into yellow. The diluted suspension was stirred at 98 °C for one day. Then, 50 mL of 30% H_2O_2 was added to the mixture. For purification, the mixture was washed by rinsing and centrifugation with 5% HCl followed by deionized (DI) water for several times. After filtration and drying under vacuum, GO was obtained as a solid.

2.3. Preparation of graphene nanosheet (GNS)/magnetite (Fe_3O_4) composite

In a typical synthesis, the as-prepared GO (0.5 g) was exfoliated by ultrasonication in 80 mL of EG for more than 3 h. 1.6 g $FeCl_3{\cdot}6H_2O$ and 3.2 g NaAc were then dissolved in GO EG solution at ambient temperature. After stirring for about 30 min, the solution was transferred into a 100 mL Teflon-lined stainless-steel autoclave and kept at 200 °C for 6 h followed by cooling to ambient temperature naturally. The black precipitate was centrifuged, washed with ethanol several times, and finally dried at 60 °C in a vacuum oven. For comparison, the AC/Fe_3O_4 composite and MWCNTs/Fe_3O_4 composite were also synthesized under the same condition by replacing AC or MWCNTs with GO.

2.4. Characterization

The powder X-ray diffraction (XRD) measurements were recorded on a Rigaku Dmax/Ultima IV diffractometer with monochromatized Cu Kα radiation (λ = 0.15418 nm). The morphology was observed with a JSM-6510 scanning electron microscope (SEM). X-ray photoelectron spectroscopy (XPS) measurements were recorded on a Perkin-Elmer PHI 5000C spectrometer using monochromatized Al Kα excitation. All binding energies were calibrated by using the contaminant carbon (C1S = 284.6 eV) as a reference. Magnetization measurements were carried out using a vibrating sample magnetometer (VSM, Lakeshore 7404) under applied magnetic field at room temperature. The leached Fe concentration in the supernatant was determined by a WFX-120 atomic absorption spectroscopy (AAS, Rayleigh Analytical Instrument Corp., China).

2.5. Adsorption of methylene blue (MB)

The adsorption of MB in aqueous solution on the as-prepared GNS/Fe_3O_4 composite was performed in a batch experiment. 0.01 g of the composite adsorbent was added into 25 mL of MB solutions of desired initial concentrations (10–25 mg L^{-1}) under stirring. At predetermined time intervals, the samples were removed from the solution by magnetic separation. The effect of pH on adsorption of MB on the composite adsorbent was studied over a pH range of 2.0–11.0 with a contact time of 20 min. The pH was adjusted by adding aqueous solutions of 0.1 mol L^{-1} HCl or 0.1 mol L^{-1} NaOH. The effect of temperature on the adsorption of MB on the composite adsorbent was investigated by determining the adsorption isotherms at 298, 308 and 318 K. The concentrations of dye were determined by using a Shimadzu UV-2550 UV–vis spectrophotometer. The amount of MB adsorbed per unit mass of the adsorbent was evaluated by using the mass balance equation:

$$q = \frac{(C_0 - C_e)V}{m} \quad (1)$$

where q (mg g^{-1}) is the amount adsorbed per gram of adsorbent, C_0 and C_e are the initial and equilibrium concentrations of MB in the solution (mg L^{-1}), respectively, m is the mass of the adsorbent used (g), and V (L) is the initial volume of the MB solution.

2.6. Desorption experiments

For the desorption study, 0.01 g of the composite adsorbent was added to 25 mL of dye solution (15 mg L^{-1}) and the mixture

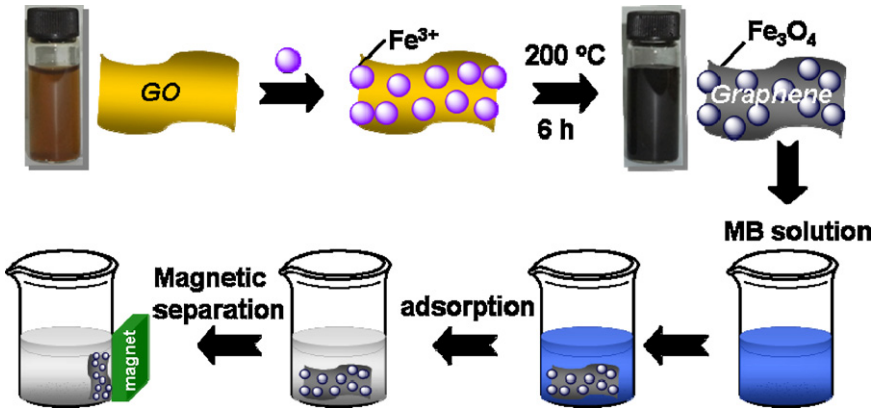

Fig. 1. Schematic illustration of the synthesis and application of the GNS/Fe_3O_4 composite.

was stirred at ambient temperature for 20 min. After the magnetic separation, the supernatant dye solution was discarded and the adsorbent alone was separated. Then, the MB-adsorbed adsorbent was added into 25 mL of ethanol and stirred for 20 min. The adsorbent was collected by a magnet and reused for adsorption again. The supernatant solutions were analyzed by UV–vis spectra. The cycles of adsorption–desorption processes were successively conducted five times.

3. Results and discussion

Fig. 1 shows a schematic illustration of the steps to synthesize GNS/Fe_3O_4 composite as a magnetically separable adsorbent for water treatment. The GO was obtained from graphite by using a modified Hummers method, which was easily suspended in EG to form a stable colloidal solution by ultrasonication, owing to its abundant surface oxygen-containing groups such as carboxyl and hydroxyl [48]. Importantly, these functional groups on GO could serve as reactive and anchoring sites for nucleation and growth of magnetic particles. During the solvothermal treatment, the added Fe^{3+} ions were *in situ* converted to Fe_3O_4 and further grew to form spherical structure; the GO was simultaneously reduced into graphene, thus resulting in the formation of the GNS/Fe_3O_4 composite. For this multifunctional structure, the graphene with two-dimensional network provided a certain amount of oxygen functionalities to create active sites for the efficient removal of dye pollutes in water [7,20,49–51]. In turn, the Fe_3O_4 attached on graphene can introduce the magnetic function to gain a facile magnetic separation from water with the help of an external magnetic field.

Fig. 2 shows the XRD patterns of the graphite, GO and solvothermal-synthesized graphene. The sharp (0 0 2) peak of the graphite at $2\theta = 26.1^\circ$ indicates an interlayer spacing of 0.34 nm. After oxidation, the characteristic graphite peak disappeared and was replaced by a well-defined peak at $2\theta = 10.8^\circ$ with 0.81 nm d-spacing. The increased d-spacing of GO sheets is due to the presence of abundant oxygen-containing functional groups on both sides of the graphene sheet causing an atomic-scale roughness on the graphene sheet. In contrast, the XRD pattern of solvothermal-synthesized graphene shows a broad peak at $2\theta = 24.4^\circ$ corresponding to an interlayer spacing of 0.36 nm, which is much lower than that of GO (0.81 nm), confirming the recovery of ordered graphitic crystal structure after solvothermal treatment. Fig. 3 shows the typical XRD patterns of the as-prepared Fe_3O_4 and GNS/Fe_3O_4 composite. In Fig. 3(a), the peaks at 2θ values of 18.2° (1 1 1), 30.0° (2 2 0), 35.3° (3 1 1), 42.9° (4 0 0), 53.4° (4 2 2), 56.9° (5 1 1), and 62.5° (4 4 0) are consistent with the standard XRD data for the cubic phase Fe_3O_4 (JCPDS no. 89-4319) with a face-centered cubic (fcc) structure. Besides these peaks, the additive peaks at 24.4° (0 0 2) corresponding to the graphene can be clearly seen from Fig. 3(b), indicating the coexistence of Fe_3O_4 and graphene in the composite.

The chemical state of element in GO and GNS/Fe_3O_4 composite were further investigated by X-ray photoelectron spectroscopy (XPS). The obtained data were calibrated by using the adventitious

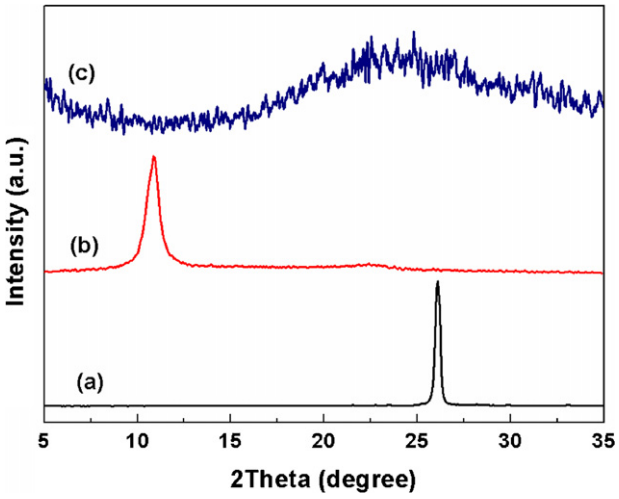

Fig. 2. XRD patterns of the graphite (a), GO (b) and graphene (c).

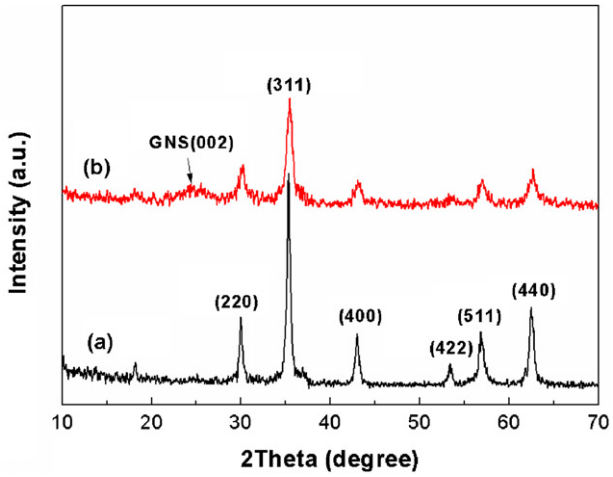

Fig. 3. XRD patterns of the Fe_3O_4 (a) and GNS/Fe_3O_4 composite (b).

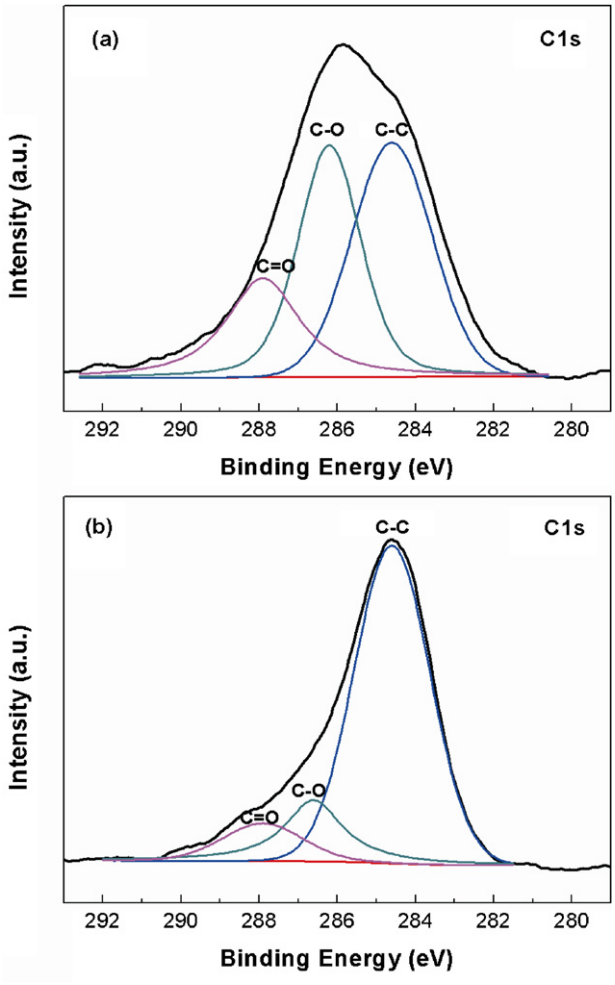

Fig. 4. C1s XPS spectra of the GO (a) and GNS/Fe_3O_4 composite (b).

carbon at a binding energy of 284.6 eV. The deconvoluted C 1s XPS spectrum of GO (Fig. 4(a)) shows three peaks at 284.6, 286.2 and 287.9 eV. The binding energy at 284.6 eV could be either assigned to the adventitious carbon contamination adsorbed from the ambient or assigned to the C–C bond (sp^2) of graphene. The peak at 286.2 eV is ascribed to the C–O bond, while the peak at 287.9 eV is assigned to the C = O bond. Compared with GO, the intensity of the C–O and C=O peaks in the GNS/Fe_3O_4 composite shown in Fig. 4(b) is dramatically decreased, suggesting that most of the oxygen-containing functional groups have been removed after reduction by EG. Hence, the chemical reduction of GO was achieved by a simple solvothermal treatment.

Scanning electron microscopy (SEM) was utilized to investigate the morphology of the as-prepared samples. Fig. 5(a,b) shows the typical SEM images of GO obtained by a modified Hummers method. The GO presents the sheet-like structure with the large thickness, smooth surface, and wrinkled edge. Interestingly, after solvothermal reduction, a significant change in morphology can be observed from Fig. 5(c,d). The obtained graphene sheets display layered structures and become very thin. The folding nature is clearly visible. The graphene sheets are exfoliated and cannot restack any more, which is consistent with the result of XRD. Fig. 6(a,b) shows the typical SEM images of the Fe_3O_4, revealing that the product consists of a large quantity of nearly uniform monodispersed spheres with the diameter of about 200 nm. After the combination with the graphene to form the GNS/Fe_3O_4 composite (Fig. 6(c,d)), the Fe_3O_4 spheres are uniformly decorated and firmly anchored on the wrinkled graphene layers with a high density. Notably, the pleats structure of the graphene may favor to hinder the Fe_3O_4 spheres from agglomeration and enable their good distribution on the graphene, while the Fe_3O_4 spheres serve as a stabilizer separate graphene sheets against the aggregation.

The magnetization measurement for the as-prepared GNS/Fe_3O_4 composite was carried out using a vibrating sample magnetometer (VSM) at room temperature with an applied magnetic field of 10 kOe. Fig. 7 shows the magnetic hysteresis loops of the as-prepared GNS/Fe_3O_4 composite, which demonstrates that the resulting composite exhibits a characteristic of ferromagnetic materials with the saturation magnetization of 42.9 emu g^{-1}, which is much lower than that of the bare Fe_3O_4 particles reported in previous literature [52]. This observed decrease in saturation magnetization reflects the standard practice of normalizing the magnetization by magnetic constituent's mass [53]. Therefore, the contribution of the nonmagnetic graphene layer to the total magnetization may be responsible for the decrease in the saturation magnetization. Meanwhile, SEM observation suggests that the magnetic Fe_3O_4 particles are intimately attached to the surface of graphene which actually acts as a magnetically inactive layer at the surface of magnetic surface in the composite system, thus affecting the uniformity or magnitude of magnetization [54]. The magnetic separability of the GNS/Fe_3O_4 composite was also tested by placing a magnet near the glass bottle. The black product is attracted toward the magnet in a short period (inset in Fig. 7), demonstrating high magnetic sensitivity of the GNS/Fe_3O_4 composite.

In recent years, considerable attention has been paid to the environmental problems involving water treatment, especially with regard to organic refractory pollutants such as organic dyes. In general, micro/nanostructured materials with the well-defined morphology and special functionality have an excellent ability to remove pollutants from water, and usually show higher removal capacities than their bulk counterparts. Meanwhile, a considerable amount of work in the literature has demonstrated that carbonaceous nanomaterials (e.g. activated carbon [55], carbon black [56], and carbon nanotube [57], etc.) could offer an attractive and inexpensive option for the efficient removal of various organic contaminants from water. Inspired by these previous results, we expect the GNS/Fe_3O_4 composite could be used as an efficient adsorbent for removal of organic pollutants. More significantly, the solid/liquid separation would be rather easy by a facile magnetic separation process under the applied external magnetic field. In this case, methylene blue (MB) was selected as a typical organic pollutant to test the ability of the GNS/Fe_3O_4 composite for adsorptive removal of organic pollutant from water.

Fig. 8 shows the time profile of MB adsorption on the GNS/Fe_3O_4 composite at different initial MB concentrations. The adsorption capacity of dye increases as the increase in the initial dye concentrations, because the more MB molecule is available at higher initial dye concentrations, and higher initial dye concentrations provide higher driving force to overcome the mass transfer resistance of the dye between the aqueous phases and the solid phases, resulting in more collisions between MB molecule and active sites on the adsorbent [58–60]. In particular, it is noteworthy that the process shows an extraordinarily fast adsorption rate, which can be verified by the fact that the amount of adsorbed MB on the GNS/Fe_3O_4 composite in a MB solution of 15 mg L^{-1} within 2 min almost achieved 64%. The fast uptake indicates the enhanced adsorption performance of the GNS/Fe_3O_4 composite for dye removal in water, which may be attributed to (i) the electrostatic attraction between the negatively charged surface oxygen-containing groups and cationic MB; (ii) the π–π interactions between the MB molecules and the aromatic rings of graphene [61]. Compared with pure GNS (Fig. 9(a)), the GNS/Fe_3O_4 composite exhibits the lower adsorption capacity

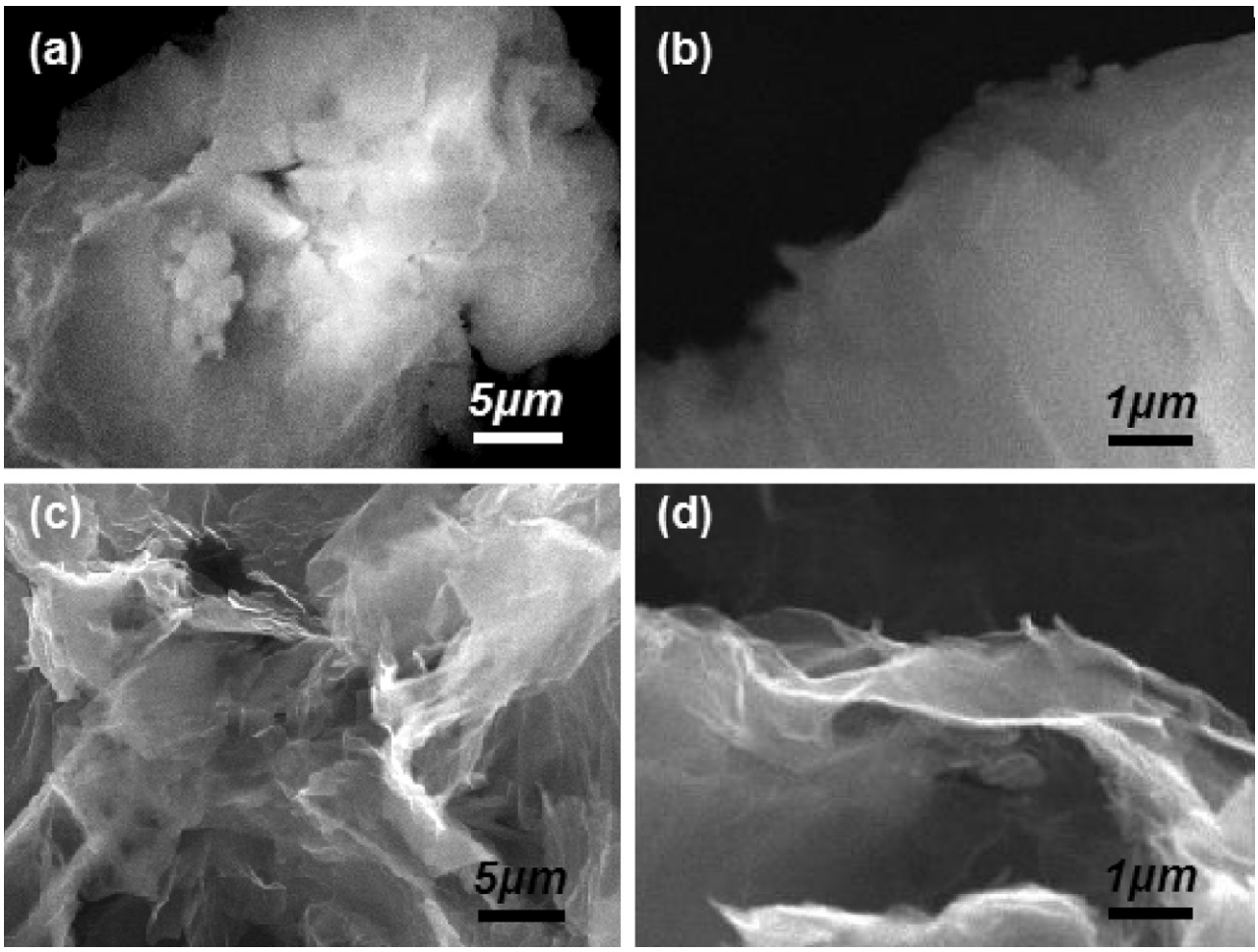

Fig. 5. SEM images of the GO (a and b) and graphene (c and d).

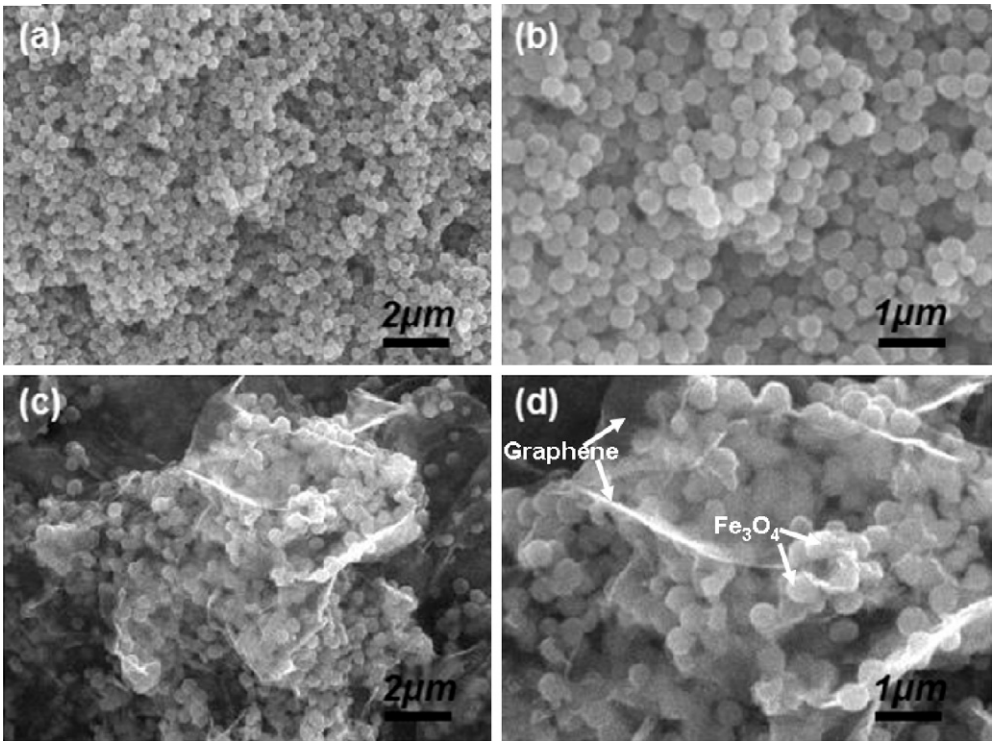

Fig. 6. SEM images of the Fe_3O_4 (a and b) and GNS/Fe_3O_4 composite (c and d).

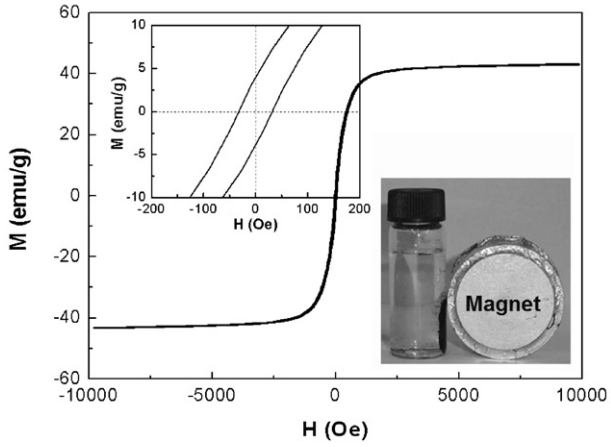

Fig. 7. Hysteresis loops of the GNS/Fe_3O_4 composite. The top inset shows close view of the hysteresis loops; the bottom inset shows the magnetic separation of the GNS/Fe_3O_4 composite under an external magnetic field.

and higher adsorption rate. Graphene is an ideal nonporous adsorbent, and adsorption mainly occurs on its planar surface which was only controlled by external diffusion [62]. The Fe_3O_4 having no ability to adsorb MB molecule (Fig. 9(a)) would occupy some active sites on the GNS, resulting in the decrease in adsorption capacity. However, it could separate graphene sheets against the aggregation proved by the result of SEM analysis (Fig. 6), which is beneficial to enhance the adsorption rate. By comparison with other magnetic carbonaceous composite, i.e., AC/Fe_3O_4 composite and MWCNTs/Fe_3O_4 composite (Fig. 9(b)), the GNS/Fe_3O_4 composite shows fast rate for MB adsorption. In addition, the adsorption capacity for MB follows the order: AC/Fe_3O_4 composite > GNS/Fe_3O_4 composite > MWCNTs/Fe_3O_4 composite. Therefore, considering relatively high adsorption capacity, rapid adsorption rate, and convenient magnetic separability of the GNS/Fe_3O_4 composite, it could be used as a promising alternative adsorbent for dye removal from water.

To well-understand the adsorption mechanism and kinetics, the pseudo-first-order and pseudo-second-order kinetic models were used to investigate the kinetics of MB adsorption on the GNS/Fe_3O_4 composite [63,64].

$$\text{Pseudo-first-order model :} \qquad \log(q_e - q_t) = \log q_e - \frac{k_1 t}{2.303} \quad (2)$$

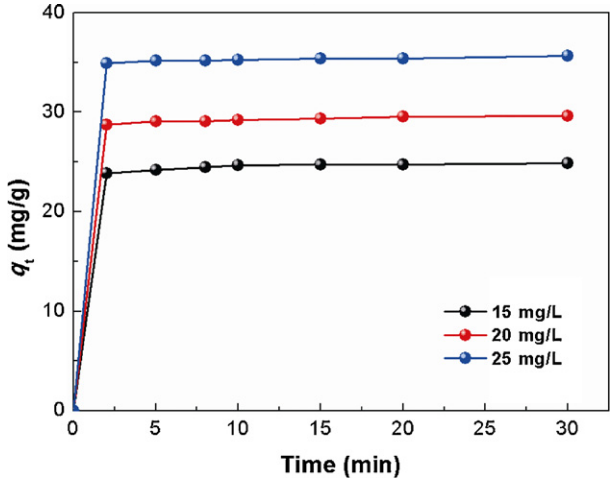

Fig. 8. Time profile of MB adsorption on the GNS/Fe_3O_4 composite with different initial MB concentrations at 25 °C.

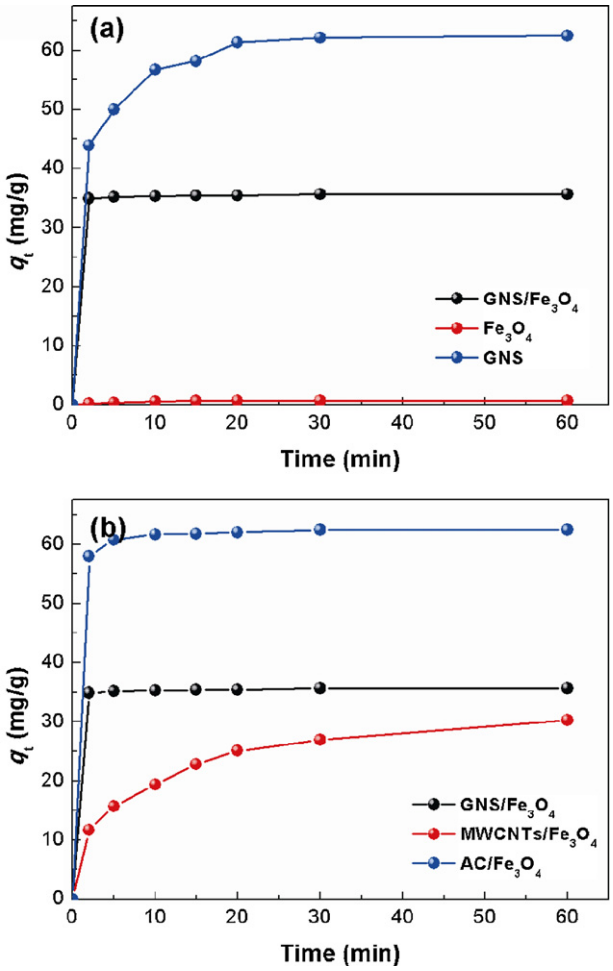

Fig. 9. Time profile of MB adsorption on different adsorbents with an initial MB concentration of 25 mg L^{-1} at 25 °C.

$$\text{Pseudo-second-order model :} \qquad \frac{t}{q_t} = \frac{1}{k_2 q_e^2} + \frac{t}{q_e} \quad (3)$$

where q_e and q_t are the amounts of MO adsorbed (mg g^{-1}) at equilibrium and at any time t (min), t is the adsorption time (min), k_1 (min^{-1}) and k_2 (g mg^{-1} min^{-1}) are the pseudo-first and pseudo-second orders rate constant, respectively. Table 1 summarizes the kinetic constants obtained by linear regression for the two models (Fig. 10). The correlation coefficients (R^2) for the pseudo-first-order model are relatively low, and the calculated q_e values ($q_{e,cal}$) from the pseudo-first-order model do not agree with the experimental data ($q_{e,exp}$), suggesting that the MB adsorption on the GNS/Fe_3O_4 composite cannot be explained a pseudo-first-order model. Actually, in many cases the pseudo-first-order equation does not fit well to the whole range of contact time and is generally applicable over the initial stage of the adsorption processes [65]. In contrast, for the pseudo-second-order model, the $q_{e,cal}$ values agree very well with the experimental ones, showing a good linearity with R^2 above 0.999. Therefore, the adsorption kinetic follows the pseudo-second-order model.

Isotherms studies can describe how the adsorbates interact with adsorbents, affording the most important parameter for designing a desired adsorption system. The adsorption isotherms of MB on the GNS/Fe_3O_4 composite at different initial concentrations are given in Fig. 11, and the equilibrium adsorption data were analyzed by the well-known Langmuir and Freundlich isotherm models [66,67]. The Langmuir isotherm is often applicable to a homogeneous adsorption surface with all the adsorption sites having equal

Table 1
Adsorption kinetic parameters for MB adsorption on the GNS/Fe_3O_4 composite.

C_0 (mg L^{-1})	Pseudo-first-order kinetics				Pseudo-second-order kinetics		
	k_1 (min^{-1})	$q_{e,cal}$ (mg g^{-1})	$q_{e,exp}$ (mg g^{-1})	R^2	k_2 (g mg^{-1} min^{-1})	$q_{e,cal}$ (mg g^{-1})	R^2
15	0.1179	0.97	24.70	0.7838	0.3191	24.91	1
20	0.1707	1.61	29.56	0.8228	0.2624	29.70	1
25	0.0574	0.78	35.42	0.9292	0.2665	35.73	0.9999

adsorbate affinity, while the Freundlich isotherm model assumes heterogeneity of adsorption surfaces, which can be expressed as

$$\text{Langmuir isotherm}: \quad \frac{C_e}{q_e} = \frac{1}{bq_m} + \frac{C_e}{q_m} \tag{4}$$

$$\text{Freundlich isotherm}: \quad \log q_e = \log K_f + \frac{1}{n} \log C_e \tag{5}$$

where q_e is the amount adsorbed at equilibrium (mg g^{-1}), C_e is the equilibrium concentration of the MB (mg L^{-1}), constant b is related to the energy of adsorption (L mg^{-1}), q_m is the Langmuir monolayer adsorption capacity (mg g^{-1}), K_f is roughly an indicator of the adsorption capacity, and $1/n$ is the adsorption intensity. Table 2 summarizes the Langmuir and Freundlich constants and the calculated coefficients. It can be found that the regression coefficient R^2 obtained from Langmuir model is much higher than that from Freundlich model, suggesting that the Langmuir isotherm fits better with the experimental data. The maximum monolayer adsorption capacity (q_m) of the GNS/Fe_3O_4 composite was calculated to be 43.82 mg g^{-1}. Moreover, the essential feature of the Langmuir isotherm can be expressed in terms of a dimensionless constant separation factor (R_L) given by the following equation [68]:

$$R_L = \frac{1}{1 + bC_0} \tag{6}$$

where b (L mg^{-1}) is the Langmuir constant and C_0 (mg L^{-1}) is the initial concentration in the liquid phase. The value of R_L indicates the shape of the isotherm to be either unfavorable ($R_L > 1$), linear ($R_L = 1$), favorable ($0 < R_L < 1$) or irreversible ($R_L = 0$) [69]. The R_L values between 0 and 1 indicate favorable adsorption. For MB adsorption on the GNS/Fe_3O_4 composite, R_L values obtained are in the range of 0.1195–0.2534, thereby confirming that the adsorption is a favorable process.

The thermodynamic studies provide in-depth information on inherent energetic changes that are associated with adsorption. In the present study, the effect of temperature on MB adsorption over the GNS/Fe_3O_4 composite was investigated, and the related thermodynamic parameters were also calculated. The thermodynamic feasibility of the adsorbent-dye interaction process can be represented as [70]

$$\Delta G^0 = -RT \ \ln K_d \tag{7}$$

where K_d is the distribution coefficient ($K_d = q_e/C_e$), ΔG^0 is the change of the Gibbs free energy, T is the temperature (K), R is the gas constant (8.3145 J mol^{-1} K^{-1}). The values of ΔG^0 are found to be negative at different temperatures, as given in Table 3, suggesting the spontaneous nature of the process. In addition, more negative value with the increase of temperature shows that the amount of MB adsorbed at equilibrium should increase with increasing temperature. Furthermore, the values of the enthalpy change (ΔH^0) and the entropy change (ΔS_0) associated with the processes were calculated using the following equations [71]:

$$\ln K_d = \frac{\Delta S^0}{R} - \frac{\Delta H^0}{RT} \tag{8}$$

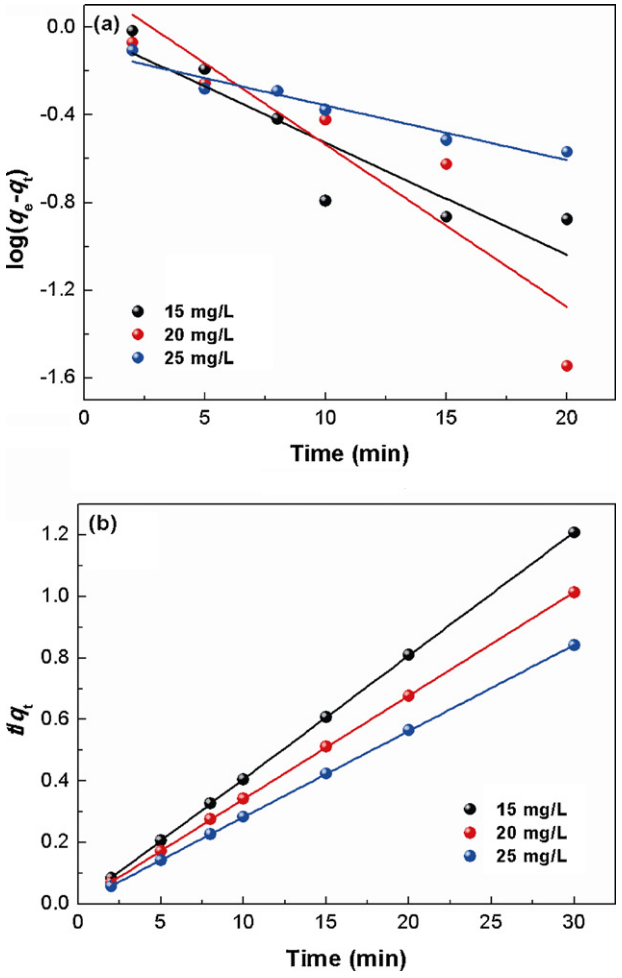

Fig. 10. Pseudo-first-order kinetics (a) and pseudo-second-order kinetics (b) of MB adsorption on the GNS/Fe_3O_4 composite.

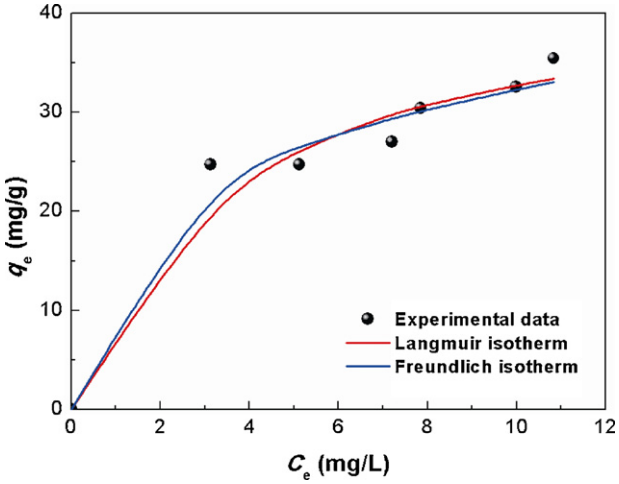

Fig. 11. Isotherms of MB adsorption on the GNS/Fe_3O_4 composite (temperature: 25 °C; contact time: 20 min).

Table 2
Adsorption isotherm parameters for MB adsorption on the GNS/Fe_3O_4 composite.

Langmuir isotherm			Freundlich isotherm		
b (L mg^{-1})	q_m (mg g^{-1})	R^2	K_f	n	R^2
0.2946	43.82	0.9132	16.56	3.4521	0.7534

Table 3
Adsorption thermodynamic parameters for MB adsorption on the GNS/Fe_3O_4 composite.

ΔH^0 (kJ mol^{-1})	ΔS^0 (J mol^{-1} K^{-1})	ΔG^0 (kJ mol^{-1})		
		298 K	308 K	318 K
22.59	88.96	−3.90	−4.84	−5.67

Therefore, the values of ΔS^0 and ΔH^0 were calculated from the slope and intercept of van't Hoff plot ($\ln K_d$ vs. $1/T$) shown in Fig. 12. The positive value of ΔH^0 indicates an endothermic nature of adsorption, while the positive value of ΔS_0 reflects an increase in randomness at the solid/solution interface during the adsorption process.

Fig. 13 shows the effect of the initial pH on the adsorption capacity of MB on the GNS/Fe_3O_4 composite. The adsorption capacity of MB gradually increases with increasing solution pH from 2.0 to 11.0. The solution pH can affect the surface charge of the adsorbent, the degree of ionization of the different pollutants, the dissociation of functional groups on the active sites of the adsorbent as well as the structure of the dye molecule. The graphene sheets are negatively charged in solution due to the presence of the oxygen-containing groups [72,73]. The decrease in the adsorption capacity of dye at lower pH values may be due to the protons competition with the dye molecules for the available adsorption sites. As the pH increases, the electrostatic attraction between the negatively charged surface of the GNS/Fe_3O_4 composite and cationic MB molecule increases, resulting in an increase in the adsorption capacity of dye.

The stability and regeneration ability of the adsorbent is crucial for its practical application. Considering that component leaching from adsorbent to water environment may cause secondary pollution, the stability of the GNS/Fe_3O_4 composite was tested by monitoring the leached Fe content. Previous study had been demonstrated that coating by a certain shielding layer was an efficient way to inhibit the Fe leaching from Fe_3O_4 [74,75]. In this case, no leaching of Fe ions from the GNS/Fe_3O_4 composite was detected during MB adsorption at natural pH by AAS, indicating the high stability of GNS/Fe_3O_4 composite. The cycles of adsorption–desorption experiments were also carried out, as shown in Fig. 14. The adsorption capacity decreases for each new cycle after desorption with five cycles. Meanwhile, after five cycles of the desorption–adsorption, the GNS/Fe_3O_4 composite has high magnetic sensitivity under an external magnetic field, which can be collected from the solution using a magnet of 4000 Gs (inset in Fig. 14). These results show that

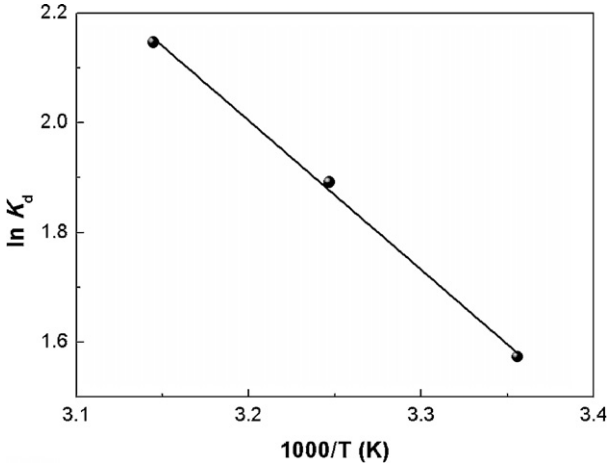

Fig. 12. Van't Hoff plot of $\ln K_d$ vs. $1/T$ (initial MB concentration: 15 mg L^{-1}; contact time: 20 min).

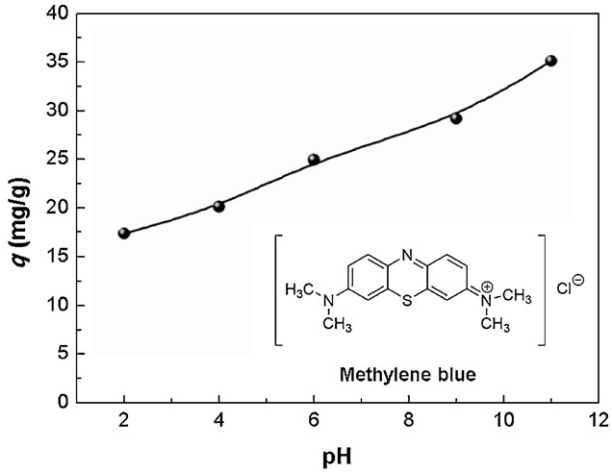

Fig. 13. Effect of solution pH on the adsorption of MB on the GNS/Fe_3O_4 composite (initial MB concentration: 15 mg L^{-1}; temperature: 25 °C; contact time: 20 min).

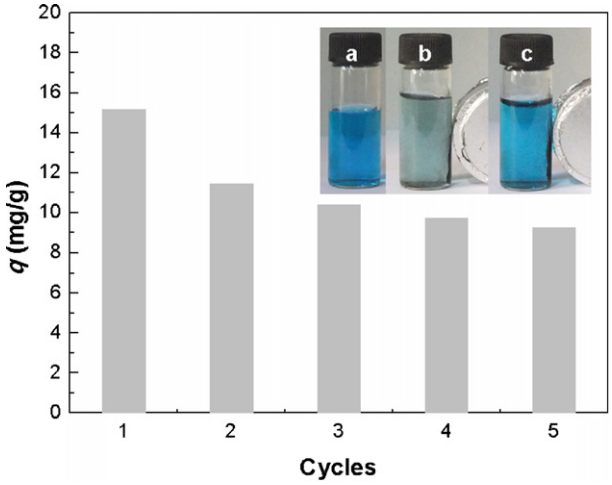

Fig. 14. Adsorption capacity of MB on the GNS/Fe_3O_4 composite in five successive cycles of desorption–adsorption (initial MB concentration: 15 mg L^{-1}; temperature: 25 °C; contact time: 20 min). Inset in figure shows photographs of aqueous solutions of MB (a) before adsorption, (b) after adsorption and (c) after fifth cycles of desorption–adsorption.

the GNS/Fe_3O_4 composite can be potentially used as a magnetic adsorbent to remove dye contaminants from water.

4. Conclusions

In conclusion, the GNS/Fe_3O_4 composite with highly efficient adsorption performance has been successfully and directly produced via a facile one-step solvothermal method. The reaction process involved *in situ* conversion of $FeCl_3$ to Fe_3O_4 and simultaneous reduction of GO into graphene in ethylene glycol solution. The resulting composite combined the both features of Fe_3O_4 and graphene, and thus exhibited extraordinary removal capacity and fast adsorption rates for MB dye removal in water, due to the electrostatic attraction between the negative surface oxygen-containing groups and cationic MB and the π–π interactions between the MB molecules and the aromatic rings of graphene. The adsorption kinetics, isotherms and thermodynamics were investigated in detail. The kinetic study revealed the adsorption process followed the pseudo-second-order kinetic model. The equilibrium data were well-modeled by the Langmuir isotherm model. The thermodynamic parameters suggested that the adsorption process was spontaneity and endothermic in nature. This study showed that the as-prepared GNS/Fe_3O_4 composite could be utilized as a magnetically separable and efficient adsorbent for the environmental cleanup.

Acknowledgments

This work was supported by Program for Scientific and Technological Innovative Team in Sichuan Provincial Universities (2010008), Open Project of Chemical Synthesis and Pollution Control Key Laboratory of Sichuan Province (11CSPC-(1-7)) and Program for Scientific Research Innovation Team of China West Normal University. Dr. Fang Liao and Prof. Yunwen Liao in China West Normal University are gratefully acknowledged for their help in XRD and SEM measurements.

References

[1] A.K. Geim, K.S. Novoselov, The rise of graphene, Nat. Mater. 6 (2007) 183–191.
[2] Y. Kopelevich, P. Esquinazi, Graphene physics in graphite, Adv. Mater. 19 (2007) 4559–4563.
[3] X.L. Li, X.R. Wang, L. Zhang, S.W. Lee, H.J. Dai, Chemically derived, ultrasmooth graphene nanoribbon semiconductors, Science 319 (2008) 1229–1232.
[4] C. Stampfer, E. Schurtenberger, F. Molitor, J. Guttinger, T. Ihn, K. Ensslin, Tunable graphene single electron transistor, Nano Lett. 8 (2008) 2378–2383.
[5] M.D. Stoller, S.J. Park, Y.W. Zhu, J.H. An, R.S. Ruoff, Graphene-based ultracapacitors, Nano Lett. 8 (2008) 3498–3502.
[6] J.C. Liu, H.W. Bai, Y.J. Wang, Z.Y. Liu, X.W. Zhang, D.D. Sun, Self-assembling TiO_2 nanorods on large graphene oxide sheets at a two-phase interface and their anti-recombination in photocatalytic applications, Adv. Funct. Mater. 20 (2010) 4175–4181.
[7] K. Haubner, J. Murawski, P. Olk, L.M. Eng, C. Ziegler, B. Adolphi, E. Jaehne, The route to functional graphene oxide, Chem. Phys. Chem. 11 (2010) 2131–2139.
[8] M.J. McAllister, J. Li, D.H. Adamson, H.C. Schnapps, A.A. Abdul, J. Liu, M.D. Herrera-Alonzo, L. Milieus, R. Car, R.K. Prud'homme, I.A. Assay, Single sheet functionalized graphene by oxidation and thermal expansion of graphite, Chem. Mater. 19 (2007) 4396–4404.
[9] S. Stankovich, D.A. Dikin, R.D. Piner, K.A. Kohlhaas, A. Kleinhammes, Y.Y. Jia, Y. Wu, S.T. Nguyen, R.S. Ruoff, Synthesis of graphene-based nanosheets via chemical reduction of exfoliated graphite oxide, Carbon 45 (2007) 1558–1565.
[10] H.L. Wang, L.F. Cui, Y. Yang, H.S. Casalongue, J.T. Robinson, Y.Y. Liang, Y. Cui, H.J. Dai, Mn_3O_4-graphene hybrid as a high-capacity anode material for lithium ion batteries, J. Am. Chem. Soc. 132 (2010) 13978–13980.
[11] C.X. Guo, H.B. Yang, Z.M. Sheng, Z.S. Lu, Q.L. Song, C.M. Li, Layered graphene/quantum dots for photovoltaic devices, Angew. Chem. Int. Ed. 49 (2010) 3014–3017.
[12] H.L. Wang, H.S. Casalongue, Y.Y. Liang, H.J. Dai, $Ni(OH)_2$ nanoplates grown on graphene as advanced electrochemical pseudocapacitor materials, J. Am. Chem. Soc. 132 (2010) 7472–7477.
[13] H. Zhang, X.J. Lv, Y.M. Li, Y. Wang, J.H. Li, P25-graphene composite as a high performance photocatalyst, ACS Nano 4 (2010) 380–386.
[14] T.G. Xu, L.W. Zhang, H.Y. Cheng, Y.F. Zhu, Significantly enhanced photocatalytic performance of ZnO via graphene hybridization and the mechanism study, Appl. Catal. B 10 (2011) 382–387.
[15] Y.H. Ng, A. Iwase, A. Kudo, R. Amal, Reducing graphene oxide on a visible-light $BiVO_4$ photocatalyst for an enhanced photoelectrochemical water splitting, J. Phys. Chem. Lett. 1 (2010) 2607–2612.
[16] E.P. Gao, W.Z. Wang, M. Shang, J.H. Xu, Synthesis and enhanced photocatalytic performance of graphene–Bi_2WO_6 composite, Phys. Chem. Chem. Phys. 13 (2011) 2887–2893.
[17] F. Caruso, M. Spasova, A. Susha, M. Giersig, R.A. Caruso, Magnetic nanocomposite particles and hollow spheres constructed by a sequential layering approach, Chem. Mater. 13 (2001) 109–116.
[18] M.P. Pileni, Magnetic fluids: fabrication magnetic properties, and organization of nanocrystals, Adv. Funct. Mater. 5 (2001) 323–336.
[19] J.Z. Wang, C. Zhong, D. Wexler, N.H. Idris, Z.X. Wang, L.Q. Chen, H.K. Liu, Graphene-encapsulated Fe_3O_4 nanoparticles with 3d laminated structure as superior anode in lithium ion batteries, Chem. Eur. J. 17 (2011) 661–667.
[20] J.J. Liang, Y.F. Xu, D. Sui, L. Zhang, Y. Huang, Y.F. Ma, F.F. Li, Y.S. Chen, Flexible, magnetic, and electrically conductive graphene/Fe_3O_4 paper and its application for magnetic-controlled switches, J. Phys. Chem. C 114 (2010) 17465–17471.
[21] H.K. He, C. Gao, Supraparamagnetic, conductive, and processable multifunctional graphene nanosheets coated with high-density Fe_3O_4 nanoparticles, ACS Appl. Mater. Interfaces 2 (2010) 3201–3210.
[22] K.F. Zhou, Y.H. Zhu, X.L. Yang, C.Z. Li, One-pot preparation of graphene/Fe_3O_4 composites by a solvothermal reaction, New J. Chem. 34 (2010) 2950–2955.
[23] B.J. Li, H.Q. Cao, J. Shao, M.Z. Qu, J.H. Warner, Superparamagnetic Fe_3O_4 nanocrystals@graphene composites for energy storage devices, J. Mater. Chem. 21 (2011) 5069–5975.
[24] X.Y. Yang, Y.S. Wang, X. Huang, Y.F. Ma, Y. Huang, R.C. Yang, H.Q. Duan, Y.S. Chen, Multi-functionalized graphene oxide based anticancer drug-carrier with dual-targeting function and pH-sensitivity, J. Mater. Chem. 21 (2011) 3448–3454.
[25] K.F. Zhou, Y.H. Zhu, X.L. Yang, C.Z. Li, Preparation and application of mediator-free H_2O_2 biosensors of graphene–Fe_3O_4 composites, Electroanalysis 23 (2011) 862–869.
[26] V.K. Gupta, P.J.M. Carrott, M.M.L. Ribeiro Carrott, Suhas, Low cost adsorbents: growing approach to wastewater treatment – a review, Crit. Rev. Environ. Sci. Technol. 39 (2009) 783–842.
[27] I. Ali, V.K. Gupta, Advances in water treatment by adsorption technology, Nat. Protoc. 1 (2006) 2661–2667.
[28] V.K. Gupta, R. Jain, S. Malath, A. Nayak, Adsorption–desorption studies of indigocarmine from industrial effluents by using deoiled mustard and its comparison with charcoal, J. Colloid Interface Sci. 348 (2010) 628–633.
[29] R. Jain, S. Sikarwar, Adsorption and desorption studies on hazardous dye Napthol Yellow S, J. Hazard. Mater. 182 (2010) 749–756.
[30] A. Mittal, J. Mittal, A. Malviya, V.K. Gupta, Removal and recovery of Chrysoidine Y from aqueous solutions by waste materials, J. Colloid Interface Sci. 344 (2010) 497–507.
[31] V.K. Gupta, A. Mittal, A. Malviya, J. Mittal, Adsorption of Carmoisine A from wastewater using waste materials-bottom ash and de-oiled soya, J. Colloid Interface Sci. 335 (2009) 24–33.
[32] V.K. Gupta, A. Mittal, R. Jain, M. Mathur, S. Sikarwar, Adsorption of safranin-T from wastewater using waste materials-activated carbon and activated rice husks, J. Colloid Interface Sci. 303 (2006) 80–86.
[33] V.K. Gupta, A. Mittal, L. Kurup, J. Mittal, Adsorption of a hazardous dye, erythrosine, over hen feathers, J. Colloid Interface Sci. 304 (2006) 52–57.
[34] V.K. Gupta, I. Ali, V.K. Saini, T.V. Gerven, B.V. derBruggen, C. Vandecasteele, Removal of dyes from waste water using bottom ash, Ind. Eng. Chem. Res. 44 (2005) 3655–3664.
[35] V.K. Gupta, Suhas, I. Ali, V.K. Saini, Removal of rhodamine B, fast green and methylene blue from wastewater using red mud, an aluminum industry waste, Ind. Eng. Chem. Res. 43 (2004) 1740–1747.
[36] V.K. Gupta, B. Gupta, A. Rastogi, S. Agarwal, A. Nayak, A comparative investigation on adsorption performances of mesoporous activated carbon prepared from waste rubber tire and activated carbon for a hazardous azo dye-Acid Blue 113, J. Hazard. Mater. 186 (2011) 891–901.
[37] V.K. Gupta, Suhas, Application of low cost adsorbents for dye removal – a review, J. Environ. Manage. 90 (2009) 2313–2342.
[38] V.K. Gupta, A. Mittal, L. Krishnan, J. Mittal, Adsorption treatment and recovery of the hazardous dye, brilliant blue FCF, over bottom ash and de-oiled soya, J. Colloid Interface Sci. 293 (2006) 16–26.
[39] V. Gupta, I. Ali, Removal of endosulfan and methoxychlor from water on carbon slurry, Environ. Sci. Technol. 42 (2008) 766–770.
[40] V.K. Gupta, A. Mittal, V. Gajbe, J. Mittal, Adsorption of basic fuchsin using waste materials-bottom ash and de-oiled soya as adsorbents, J.Colloid Interface Sci. 319 (2008) 30–39.
[41] L.H. Ai, H.Y. Huang, Z.L. Chen, X. Wei, J. Jiang, Activated carbon/$CoFe_2O_4$ composites: facile synthesis, magnetic performance and their potential application for the removal of malachite green from water, Chem. Eng. J. 156 (2010) 243–249.
[42] L.C.A. Oliveira, R.V.R.A. Rios, J.D. Fabris, V. Garg, K. Sapag, R.M. Lago, Activated carbon/iron oxide magnetic composites for the adsorption of contaminants in water, Carbon 40 (2002) 2177–2183.
[43] X.J. Peng, Z.K. Luan, Z.C. Di, Z.G. Zhang, C.L. Zhu, Carbon nanotubes–iron oxides magnetic composites as adsorbent for removal of Pb(II) and Cu(II) from water, Carbon 43 (2005) 880–883.

[44] A.K. Mishra, S. Ramaprabhu, Magnetite decorated multiwalled carbon nanotube based supercapacitor for arsenic removal and desalination of seawater, J. Phys. Chem. C 114 (2010) 2583–2590.
[45] V. Chandra, J. Park, Y. Chun, J.W. Lee, I.C. Hwang, K.S. Kim, Water-dispersible magnetite-reduced graphene oxide composites for arsenic removal, ACS Nano 4 (2010) 3979–3986.
[46] H.Y. Koo, H.J. Lee, H.A. Go, Y.B. Lee, T.S. Bae, J.K. Kim, W.S. Choi, Graphene-based multifunctional iron oxide nanosheets with tunable properties, Chem. Eur. J. 17 (2011) 1214–1219.
[47] C.M. Chen, Q.H. Yang, Y.G. Yang, W. Lv, Y.F. Wen, P.X. Hou, M.Z. Wang, H.M. Cheng, Self-assembled free-standing graphite oxide membrane, Adv. Mater. 21 (2009) 3007–3011.
[48] D.R. Dreyer, S. Park, C.W. Bielawski, R.S. Ruoff, The chemistry of graphene oxide, Chem. Soc. Rev. 39 (2010) 228–240.
[49] B. Das, B. Choudhury, A. Gomathi, A.K. Manna, S.K. Pati, C.N.R. Rao, Interaction of inorganic nanoparticles with graphene, Chem. Phys. Chem. 12 (2011) 937–943.
[50] G.X. Wang, B. Wang, X.L. Wang, J. Park, S.X. Dou, H. Ahn, K. Kim, Sn/graphene nanocomposite with 3D architecture for enhanced reversible lithium storage in lithium ion batteries, J. Mater. Chem. 19 (2009) 8378–8384.
[51] L.F. Shen, C.Z. Yuan, H.J. Luo, X.G. Zhang, S.D. Yang, X.J. Lu, In situ synthesis of high-loading $Li_4Ti_5O_{12}$–graphene hybrid nanostructures for high rate lithium ion batteries, Nanoscale 3 (2011) 572–574.
[52] H. Deng, X.L. Li, Q. Peng, X. Wang, J.P. Chen, Y.D. Li, Monodisperse magnetic single-crystal ferrite microspheres, Angew. Chem. Int. Ed. 44 (2005) 2782–2785.
[53] C.R. Vestal, Z.J. Zhang, Synthesis and magnetic characterization of Mn and Co spinel ferrite–silica nanoparticles with tunable magnetic core, Nano Lett. 3 (2003) 1739–1743.
[54] S. Rana, J. Rawat, R.D.K. Misra, Anti-microbial active composite nanoparticles with magnetic core and photocatalytic shell: TiO_2-$NiFe_2O_4$ biomaterial system, Acta Biomater. 1 (2005) 691–703.
[55] D. Mohan, C.U.J. Pittman Jr., Activated carbons and low cost adsorbents for remediation of tri- and hexavalent chromium from water, J. Hazard. Mater. 137 (2006) 762–811.
[56] M. Bele, A. Kodre, I. Arcon, J. Grdadolnik, S. Pejovnik, J.O. Besenhard, Adsorption of cetyltrimethylammonium bromide on carbon black from aqueous solution, Carbon 36 (1998) 1207–1212.
[57] V.K. Upadhyayula, S.G. Deng, M.C. Mitchell, G.B. Smith, Application of carbon nanotube technology for removal of contaminants in drinking water: a review, Sci. Total Environ. 408 (2009) 1–13.
[58] B.H. Hameed, A.A. Ahmad, N. Aziz, Adsorption of reactive dye on palm-oil industry waste: equilibrium, kinetic and thermodynamic studies, Desalination 247 (2009) 551–560.
[59] M. Ghaedi, A. Hassanzadeh, S.N. Kokhdan, Multiwalled carbon nanotubes as adsorbents for the kinetic and equilibrium study of the removal of alizarin red S and morin, J. Chem. Eng. Data 56 (2011) 2511–2520.
[60] L.H. Ai, J. Jiang, Fast removal of organic dyes from aqueous solutions by AC/ferrospinel composite, Desalination 262 (2010) 134–140.
[61] F.H. Li, Y. Bao, J. Chai, Q.X. Zhang, D.X. Han, L. Niu, Synthesis and application of widely soluble graphene sheets, Langmuir 26 (2010) 12314–12320.
[62] Z.-H. Huang, X.Y. Zheng, W. Lv, M. Wang, Q.-H. Yang, F.Y. Kang, Adsorption of lead(II) ions from aqueous solution on low-temperature exfoliated graphene nanosheets, Langmuir 27 (2011) 7558–7562.
[63] S. Lagergren, About the theory of so-called adsorption of soluble substances, Kungliga Svenska Vetenskapsakademiens Handlingar 24 (1898) 1–39.
[64] Y.S. Ho, G. McKay, Sorption of dye from aqueous solution by peat, Chem. Eng. J. 70 (1998) 115–124.
[65] G. McKay, Y.S. Ho, The sorption of lead (II) on peat, Water Res. 33 (1999) 578–584.
[66] I. Langmuir, The Constitution and fundamental properties of solids and liquids, J. Am. Chem. Soc. 38 (1916) 2221–2295.
[67] H.M.F. Freundlich, Over the adsorption in solution, Z Phys. Chem. 57 (1906) 385–471.
[68] T.W. Weber, R.K. Chakravorti, Pore and solid diffusion models for fixed-bed adsorbers, AIChE J. 20 (1974) 228–238.
[69] G. McKay, Adsorption of dyestuffs from aqueous solution with activated carbon. I. Equilibrium and batch contact time studies, J. Chem. Technol. Biotechnol. 32 (1982) 759–772.
[70] A. Sarı, M. Tuzen, Biosorption of Pb(II) and Cd(II) from aqueous solution using green alga (Ulva lactuca) biomass, J. Hazard. Mater. 152 (2008) 302–308.
[71] B.H. Hameed, A.A. Ahmad, Batch adsorption of methylene blue from aqueous solution by garlic peel, an agricultural waste biomass, J. Hazard. Mater. 164 (2009) 870–875.
[72] H. Kim, S.W. Kim, Y.U. Park, H. Gwon, D.H. Seo, Y. Kim, K. Kang, SnO_2/graphene composite with high lithium storage capability for lithium rechargeable batteries, Nano Res. 3 (2010) 813–821.
[73] T.H. Han, W.J. Lee, D.H. Lee, J.E. Kim, E.Y. Choi, S.O. Kim, Peptide/graphene hybrid assembly into core/shell nanowires, Adv. Mater. 22 (2010) 2060–2064.
[74] J.-F. Liu, Z.-S. Zhao, G.-B. Jiang, Coating Fe_3O_4 magnetic nanoparticles with humic acid for high efficient removal of heavy metals in water, Environ. Sci. Technol. 42 (2008) 6949–6954.
[75] J.H. Wang, S.R. Zheng, Y. Shao, J.L. Liu, Z.Y. Xu, D.Q. Zhu, Amino-functionalized Fe_3O_4@SiO_2 core-shell magnetic nanomaterial as a novel adsorbent for aqueous heavy metals removal, J. Colloid Interface Sci. 349 (2010) 293–299.